Nonrenewal Statistics of Electrosensory Afferent Spike Trains: Implications for the Detection of Weak Sensory Signals

Rama Ratnam[1,2] and **Mark E. Nelson**[1,2]

[1]*Department of Molecular and Integrative Physiology, and* [2]*Beckman Institute, University of Illinois at Urbana-Champaign, Urbana, Illinois 61801*

The ability of an animal to detect weak sensory signals is limited, in part, by statistical fluctuations in the spike activity of sensory afferent nerve fibers. In weakly electric fish, probability coding (P-type) electrosensory afferents encode amplitude modulations of the fish's self-generated electric field and provide information necessary for electrolocation. This study characterizes the statistical properties of baseline spike activity in P-type afferents of the brown ghost knifefish, *Apteronotus leptorhynchus.* Short-term variability, as measured by the interspike interval (ISI) distribution, is moderately high with a mean ISI coefficient of variation of 44%. Analysis of spike train variability on longer time scales, however, reveals a remarkable degree of regularity. The regularizing effect is maximal for time scales on the order of a few hundred milliseconds, which matches functionally relevant time scales for natural behaviors such as prey detection. Using high-order interval analysis, count analysis, and Markov-order analysis we demonstrate that the observed regularization is associated with memory effects in the ISI sequence which arise from an underlying nonrenewal process. In most cases, a Markov process of at least fourth-order was required to adequately describe the dependencies. Using an ideal observer paradigm, we illustrate how regularization of the spike train can significantly improve detection performance for weak signals. This study emphasizes the importance of characterizing spike train variability on multiple time scales, particularly when considering limits on the detectability of weak sensory signals.

Key words: electrosensory afferent; electrolocation; interspike interval analysis; Markov process; spike train variability; weak signal detection

Survival in an animal's natural environment is dependent on the ability to detect behaviorally relevant stimuli, such as those caused by predators and prey. Being able to reliably and efficiently detect such signals at weak levels confers a competitive advantage. Thus many sensory systems, including the electrosensory system discussed here, have presumably experienced selective pressures over the course of evolution to improve detection performance for weak sensory signals.

The decision of whether or not a stimulus is present must ultimately be based on a change in the spike activity of primary afferent nerve fibers. In many cases, this change must be detected in the presence of ongoing spontaneous activity. Intuitively, a subtle change in spike activity caused by a weak external signal should be easier to detect when the baseline activity is regular and predictable than when it is irregular and subject to random fluctuations. To understand the limits on signal detection performance, it is thus important to characterize the variability of baseline activity in primary afferent spike trains.

A common approach for characterizing spike train variability is by analysis of the first-order interspike interval (ISI) distribution (Hagiwara, 1954; Moore et al., 1966; Ratliff et al., 1968; Gabbiani and Koch, 1998). The coefficient of variation (the SD divided by the mean) of the ISI distribution provides a convenient measure of the variability in the arrival time between successive spikes. It is important to realize, however, that the first-order ISI distribution only provides information about short-term variability on time scales comparable to the mean ISI. Long-term variability, over time periods containing multiple spikes, must be measured using other techniques, such as analysis of higher-order interval distributions (Rodieck et al., 1962; Moore et al., 1966) or spike count distributions (Barlow and Levick, 1969a,b; Teich and Khanna, 1985).

Measurements of long-term variability for primary afferent spike trains are not commonly encountered in the literature. These measures would indeed be redundant if afferent spike activity could be adequately modeled as a renewal process. For a renewal process, successive intervals in the ISI sequence are independent and identically distributed (Cox, 1962) and therefore, higher-order interval and count distributions can be derived knowing only the first-order ISI distribution. Thus, variability on all time scales can be computed. However, when spike activity arises from a nonrenewal process there will be correlations and history-dependent effects in the ISI sequence. In such cases, the first-order ISI distribution does not provide sufficient information to predict long-term spike train variability or to set limits on signal detection performance.

In this paper, we analyze the variability of baseline spike activity recorded from P-type (probability coding) electrosensory afferent fibers in the weakly electric fish *Apteronotus leptorhynchus* (brown ghost knife fish). Objects near the fish that differ in impedance from the surrounding water modulate the self-generated electric field because of the fish's electric organ discharge (EOD). These modulations provide sensory cues that allow the fish to hunt and navigate in the dark using electrolocation (Rasnow, 1996) (for review, see Bullock and Heiligenberg, 1986). P-type afferents respond to the strength of amplitude modulations (AMs) by increasing or decreasing their probability of firing (Scheich et al., 1973; Bastian, 1981; for review, see Zakon, 1986). Their AM response characteristics have been well studied (Hagiwara et al., 1965; Scheich et al., 1973; Hopkins, 1976; Bastian, 1981; Shumway, 1989; Wessel et al., 1996; Xu et al., 1996; Nelson et al., 1997), but variability of baseline spike activity has not been fully characterized.

Infrared video recordings of prey capture behavior in *Apteronotus* performed in our laboratory have been used to estimate the behavioral threshold for detecting small prey (*Daphnia magna*, 2–3 mm in length) in the dark. At the time of detection, we estimate that the prey gives rise to an AM signal that transiently changes the firing probability of P-type afferents by only ~1% (Nelson and MacIver, 1999). In this study we show that P-type afferent spike trains are irregular as judged by the first-order ISI distribution but

that there is an underlying nonrenewal process that serves to make the spike train more regular over longer time intervals. In an ideal observer framework (Green and Swets, 1966) this regularity effectively reduces the detection threshold for weak stimuli, such as those caused by small prey.

MATERIALS AND METHODS

Electrophysiology

Extracellular recordings were made from isolated P-type afferent fibers of weakly electric fish *Apteronotus leptorhynchus.* Surgical and nerve recording procedures used here are identical to those described in an earlier study (Xu et al., 1996). Briefly, fish were anesthetized in 100 ppm tricaine methanesulfonate (MS-222; Sigma, St. Louis, MO) and immobilized with an intramuscular injection of 3 μl 10% gallamine triethiodide (Flaxedil; Sigma). P-type afferent fiber activity was recorded from the posterior branch of the left anterior lateral line nerve (pALLN), which innervates trunk electroreceptors. Recordings were made in the presence of the EOD of the fish with no other stimulus present. We refer to activity under these conditions as "baseline" activity, in contrast to spontaneous activity that would be obtained if the EOD were silenced. Action potentials were recorded from pALLN fibers with glass microelectrodes (impedance of 10–30 MΩ) filled with 3 M KCl solution. Neural activity and EOD waveforms were digitized at 17 kHz and stored for offline analysis. Spike events in the nerve recording were identified by a threshold criteria and time-stamped with a resolution of 60 μsec. All data analysis was performed on Sun workstations using custom software and the MATLAB programming environment (The MathWorks).

Spike train representation

Apteronotus leptorhynchus has a continuous quasi-sinusoidal EOD waveform with a fundamental frequency f that ranges from 750 to 1000 Hz depending on the individual. P-type units fire at most once per EOD cycle and randomly skip cycles between successive spikes. On average, a typical unit fires on about one-third of the EOD cycles. This ratio is referred to as the per-cycle probability of firing p. In the presence of a stimulus, the per-cycle probability is modulated by stimulus intensity, and hence P units are called probability coders.

When spike times are sampled at intervals smaller than the EOD period, the timing of spikes within the cycle can be observed. This is illustrated in the ISI histogram shown in Figure 1*A*. The peaks of the ISI distribution are separated by one EOD period. The width of each peak reflects the variability in firing phase within the EOD cycle. In subsequent analyses in this paper, we only keep information about the occurrence of a spike in an EOD cycle and discard information about the phase within the cycle. That is, we resample the spike train at the EOD frequency f. The effect of this resampling is seen in Figure 1*C*, which is the discrete time ISI histogram for the fiber shown in Figure 1*A*. Time is measured in EOD cycles and hence, ISIs assume only integer values $j \geq 1$, where j is the number of cycles to the next spike. For the remainder of this work, we only consider discrete-time spike trains sampled at the EOD rate.

The resampled spike train is a realization of a discrete time stochastic process $x(i)$ where $i \geq 1$ is the EOD cycle number. Furthermore, $x(i) = 1$ if there is a spike in cycle i and is zero otherwise. The mean per-cycle firing probability is given by $p = n/T$ where $n = \Sigma_{i=1}^T x(i)$ is the total number of spikes observed in a record of duration T EOD cycles. The stochastic process $x(i)$ can be characterized in terms of the statistical properties of the time intervals between spikes (interval analysis) or by the statistical properties of spike counts in time windows of fixed durations (count analysis) (Cox and Lewis, 1966).

Interval sequences and distributions of order k

Let t_i represent the EOD period number in which the ith spike occurs. We set the time origin to be such that $t_1 = 1$. Interval sequences of order k are defined as (Rodieck et al., 1962; Moore et al., 1966)

$$S_k(i) = t_{ki+1} - t_{k(i-1)+1}, \; 1 \leq i \leq \frac{n-1}{k}, \tag{1}$$

where n is the total number of spikes. The sequence S_k is a discrete-time stochastic process of strictly positive integers. The first-order interval sequence $S_1(i) = t_{i+1} - t_i$ is the sequence of ISIs, $S_2(i)$ is the sequence of times between every second spike, etc. Let I_k be the normalized kth order interval histogram (IH) constructed from S_k. Then $I_k(j)$ is the probability of observing an interval of length j in the sequence S_k. We denote the mean and variance of I_k by $\bar{I}_k$ and $\text{Var}(I_k)$, respectively. In this paper, interval sequences and IHs were calculated for orders k up to 4096. In the neurophysiology literature, I_1 is used extensively and is referred to as the ISI distribution. The shape and statistical properties (mean and variance) of the ISI distribution are often used to characterize firing patterns and variability of spike timing. However, the ISI provides a characterization of spike variability only on time scales comparable to the mean ISI. Higher-order interval distributions provide information about variability over longer time scales and about dependencies in the ISI sequence.

Dependency of an interval on the immediately preceding interval was analyzed using the joint interval histogram $I(j_1, j_2)$, which reflects the probability of observing an ISI of length j_1 followed by an ISI of length j_2 (Rodieck et al., 1962). The joint interval histogram is constructed from the sequence S_1 by binning all overlapping tuples $(S_1(i), S_1(i + 1))$, where $1 \leq i \leq n - 1$. Figure 1, *B* and *D*, shows plots of the joint interval histogram corresponding to the sampling resolutions of Figures 1 *A* and *C*, respectively.

Count distributions

An alternate analysis of spike train variability can be made using spike count distributions (Barlow and Levick, 1969a,b; Teich and Khanna, 1985). Proceeding as for interval analysis, count statistics were obtained from two measures: count sequences and count histograms. Let T be the number of EOD periods in which a count is to be performed. Then we define the count sequence N_T by counting the number of spikes occurring in blocks of T contiguous EOD cycles. This can be expressed as:

$$N_T(i) = \sum_{j=(i-1)T+1}^{iT} x(j), \; 1 \leq i \leq \frac{n}{T}, \tag{2}$$

where i refers to the block number in the sequence and n is the total number of recorded spikes. The normalized count histogram C_T was also calculated from N_T, so that $C_T(m)$ is the probability of obtaining m spikes in a count window of duration T EOD cycles. The mean and variance of C_T are denoted by $\bar{C}_T$ and $\text{Var}(C_T)$, respectively. Count sequences and histograms were calculated for T values ranging from 20 to as many as 50,000 EOD cycles, depending on data availability and subject to a minimum of 10 counting blocks.

Spike train models

To gain an understanding of the process that generates the observed spike train data $x(i)$, we created surrogate spike trains using three model systems that reproduce certain statistical features of the afferent data.

Binomially generated spike train (B). The classic description of a P-type afferent is that it is a "probability coder." Namely, the afferent fires irregularly with a per-cycle probability p that is constant under baseline conditions, but is subject to modulation in the presence of external stimuli. Thus, the simplest model of P-unit baseline activity is a process that emits a spike in any given EOD cycle with constant probability p independent of previous history. In a continuous-time framework, a constant firing probability per unit time gives rise to a homogeneous Poisson process, which frequently serves as a basis for models of spontaneous activity in neural spike trains (Tuckwell, 1988). In the discrete-time framework considered here, a constant firing probability per time step (one EOD cycle) gives rise to a binomial process. Whereas the Poisson process has exponentially distributed ISIs and Poisson-distributed spike counts, the binomial process has geometrically distributed ISIs and binomially distributed counts (see Eqs. 10 and 12, Appendix A). Surrogate binomial spike trains B were generated by shuffling the observed spike sequence $x(i)$ to remove all dependencies between adjacent EOD periods. Per-cycle firing probability p remains unchanged because shuffling preserves the total number of spikes and EOD periods.

Zeroth-order Markov process (M_0). The binomially generated spike train matches p but does not guarantee that the interval distributions will be the same as the data. A surrogate spike train that preserves p as well as the ISI distribution I_1, can be generated by randomly shuffling the ISI sequence S_1, rather than shuffling the spike train x. This preserves the total number of intervals and the distribution of intervals but removes dependencies between neighboring intervals in the sequence (Longtin and Racicot, 1997a). For reasons discussed below, this process will be referred to as M_0, indicating that it is a zeroth-order Markov process.

First-order Markov process (M_1). Interval distributions of experimentally observed spike trains often exhibit dependencies on prior activity and are thus nonrenewal (Kuffler et al., 1957; Werner and Mountcastle, 1963; Teich et al., 1990; Lowen and Teich, 1992). Surrogate spike trains that preserved dependencies between adjacent ISIs were constructed from the afferent data. First, all adjacent pairs of intervals (j_i, j_{i+1}) were tabulated and sorted into groups, each having identical first element. A group, say with first element j_a, was selected at random, and a tuple was drawn, say (j_a, j_b). The next tuple was drawn at random from the group which had first element j_b. If this tuple was (j_b, j_c), the resultant of the two draws was the triplet (j_a, j_b, j_c). All draws were made without replacement. Continuing in this manner, an ISI sequence was constructed that had joint probability $I(j_1, j_2)$ that matched the data. As discussed below, the resulting sequence is a first-order Markov process and will be denoted by M_1.

The binomial (B) and zeroth-order Markov (M_0) processes are examples of renewal processes (Cox, 1962) because successive intervals in the ISI sequence S_1 are independent and identically distributed. The first-order Markov process (M_1) is a nonrenewal process because intervals are not independent. Appendix A summarizes some results for renewal processes.

Measures of variability

A common measure of spike train variability is the coefficient of variation of the ISI distribution CV_I, defined as the SD of the ISI distribution divided by its mean. Because it is a dimensionless quantity, it can be used

for comparing the variability of two distributions even when they differ in their means. To measure variability of ISIs on different time scales, we also computed CV_1 for higher order interval distributions. The coefficient of variation $CV_1(k)$ for the *k*th order interval distribution I_k is:

$$CV_1(k) = \text{Var}(I_k)^{1/2}/\bar{I}_k. \tag{3}$$

Another useful measure is the variance-to-mean ratio of I_k, denoted $F_I(k)$:

$$F_I(k) = \text{Var}(I_k)/\bar{I}_k \text{ (EOD cycles).} \tag{4}$$

Although this measure has the disadvantage that it is not dimensionless, it has the useful property that for all orders *k*, it is constant for a renewal process (see Appendix B). For any process that is more regular than a renewal process, the variance-to-mean ratio decreases with increasing *k*.

Analogous to the measures of variability for interval sequences, it is possible to define similar measures for count sequences N_T. Proceeding as above, the coefficient of variation $CV_C(T)$ for the count distribution $C_T(i)$ is defined as:

$$CV_C(T) = \text{Var}(C_T)^{1/2}/\bar{C}_T. \tag{5}$$

For spike count distributions, the variance-to-mean ratio is called the Fano factor (Fano, 1947). It is denoted $F_C(T)$ and defined as:

$$F_C(T) = \text{Var}(C_T)/\bar{C}_T \text{ (spikes).} \tag{6}$$

Correlation analysis

History-dependent effects were analyzed by considering the serial correlation coefficient (SCC) ρ_l of the first-order sequence S_1, where *l* is the lag in terms of the number of intervening intervals. The ρ_l were computed from:

$$\rho_l = \frac{\sum_{i=1}^{M-l}(j_i - \bar{I}_1)(j_{i+l} - \bar{I}_1)}{(\sum_{i=1}^{M-l}(j_i - \bar{I}_1)^2 \sum_{i=1}^{M-l}(j_{i+l} - \bar{I}_1)^2)^{1/2}}, l = 0, 1, \ldots, \tag{7}$$

where $j_1, \ldots, j_M$ is a sequence of *M* consecutive ISIs that can start anywhere in the ISI sequence S_1. The values of ρ_l range from +1 (perfect correlation) to −1 (perfect anti-correlation), and $\rho_l = 0$ when intervals are uncorrelated.

To determine if the ρ_l were significantly different from zero, the sequence S_1 was divided into nonoverlapping blocks each having $M = 1000$ elements $S_1(i), \ldots, S_1(i + M - 1)$, and the ρ_l were determined for each block. The sequence S_1 was then shuffled to eliminate dependencies between intervals, if any, and the ρ_l were again evaluated for the same number of blocks *M*. For each lag, the unshuffled and shuffled SCCs were tested under the null hypothesis that the two populations were identical. A Wilcoxon rank sum test was used to test the hypothesis at a significance level of $p = 0.01$.

Analysis of Markov order

SCCs do not completely characterize dependencies between ISIs. This can be seen from Equation 7 where the SCC at lag *l* depends only on the pairs $(S_1(i), S_1 (i + l))$ but does not depend on the intervening $(l − 1)$ lags. Higher-order history-dependent effects in the interval sequence S_1 can be modeled by Markov chains (Nakahama et al., 1972; van der Heyden et al., 1998). The ISI sequence S_1 can be described by a Markov chain of order *n*, if intervals in the chain are dependent on exactly *n* preceding intervals. If the intervals are independent, the process is referred to as zero-order Markov (M_0). Examples of such processes are the binomially generated spike train (*B*) and shuffled ISI process M_0 described above. The process M_1, on the other hand, is first-order Markov because the statistics of the current interval are completely determined given the previous interval.

Consider a sequence of ISIs $\{j_m, j_{m-1}, \ldots, j_0\}$, where j_r refers to the *r*th lag relative to the current ISI j_0. For a Markov chain we can define the *m*th order transition probability as $p(j_0|j_m, \ldots, j_1)$, which is the probability of observing the interval j_0 given that we have observed the sequence $\{j_m, j_{m-1}, \ldots, j_1\}$ in the immediate past. Note that the definition of the *m*th order transition probability does not say anything about the order of the chain itself. The Markov order *n* of the chain is defined as the smallest value of *n* for which $p(j_0|j_m, \ldots, j_n, \ldots, j_1) = p(j_0|j_n, \ldots, j_1)$ for all $m \geq n$. Hereafter, we use the symbol *m* to denote the order of the transition probability, and the symbol *n* as the fixed number representing the order of the Markov chain. The transition probabilities $p(j_0|j_m, \ldots, j_1)$ can be estimated from the experimentally observed ISI sequence by counting all occurrences of j_0 immediately after the tuple $(j_m, \ldots, j_1)$.

Given an experimentally observed ISI sequence, we wish to determine the Markov order of the underlying process that generated the sequence. This can be done by comparing transition probabilities obtained from the data with transition probabilities of surrogate spike trains that are constructed to be of known Markov order. Statistical comparisons can be made using the *m*th order conditional entropy h_m as a test statistic (van der Heyden et al., 1998). The h_m are defined as:

$$h_0 = - \sum_{j_0} p(j_0)\log p(j_0), \tag{8}$$

$$h_m = - \sum_{j_m, \ldots, j_0} p(j_m, \ldots, j_1)p(j_0|j_m, \ldots, j_1)\log p(j_0|j_m, \ldots, j_1), m \geq 1, \tag{9}$$

for all possible tuples $(j_m, \ldots, j_0)$ having nonzero joint probability $p(j_m, \ldots, j_0)$. The conditional entropy satisfy $h_{m+1} \leq h_m$, for all *m* (Shannon, 1948). For an *n*th order Markov chain, $h_m = h_n$ for all $m \geq n$.

We follow the procedure of van der Heyden et al. (1998) for testing the order of a Markov chain. Hypothesis testing was performed for increasing orders *m*, beginning with $m = 0$. The null hypothesis was that the process is Markov order *m*. The alternative hypothesis was that the process is order $(m + 1)$ or greater. The test statistic was the $(m + 1)$th order conditional entropy h_{m+1} given by Equation 9. The statistic h_{m+1} was evaluated for both afferent and surrogate data sets. A total of $R_s = 49$ surrogate data sets were generated, and the rank *r* of the afferent data set was determined. Because the test is one-sided, the *p* value for the test is $p = r/(R_s + 1)$. The null hypothesis was rejected if $p \leq 0.05$.

Hypothesis testing was performed for increasing orders *m* until the null hypothesis could not be rejected or until the testing was terminated because of insufficient numbers of surrogate sequences. The criteria for terminating the test was $N_m < N/R_s$, where *N* was the number of intervals in S_1, and N_m was the number of distinct $(m + 1)$ tuples extracted from the data set. In this case only a lower-bound for the order *n* could be estimated.

Weak signal detection

The impact of spike train regularity on signal detection performance was estimated for afferents and the three matched spike train models. The detection algorithm was based on an ideal observer paradigm (Green and Swets, 1966) using spike count distributions. For each binary spike train $x(i)$ (see above), signal windows of duration 100 EOD periods were selected at regular intervals of 300 EOD periods. A random offset (uniform between 0 and 99) was added to the starting position of each signal window. A trial consisted of the addition of a constant number of spikes (n_s) to each signal window. Spikes were randomly distributed and added only in those EOD periods that did not already contain a spike. A sequence of spike counts was then generated using Equation 2 with $T = 100$ EOD periods. If the count exceeded a fixed threshold (see below) a "hit" was generated for that counting window. Because the threshold can be exceeded because of random fluctuations in the baseline even when there is no signal present, a percentage of the hits will be false alarms. Let N_s denote the total number of counting windows where signal + baseline is present, with N_{hs} of these windows receiving a hit. Similarly, let N_b denote the total number of counting windows where only baseline is present, with N_{hb} of these windows receiving a hit. Then detection probability is given by $P_d = N_{hs}/N_s$, and false alarm probability is given by $P_{fa} = N_{hb}/N_b$. The threshold was chosen such that the false alarm probability P_{fa} was 0.001 or less, motivated by the low rate of false strikes observed in our prey capture studies (Nelson and MacIver, 1999). Trials were repeated for $n_s = 1, 2, \ldots, 30$, and P_d was evaluated as a function of n_s.

RESULTS

Baseline spiking activity in the absence of any external stimulus other than the fish's ongoing EOD was recorded from 52 individual P-type afferent fibers in eight fish. The EOD frequency of an individual fish was constant and ranged from 750 to 1000 Hz. Afferent baseline record lengths ranged from 83 to 2048 sec, with a median of 428 sec. The firing rate for individual afferent fibers was nearly constant over the duration of the recording. Baseline firing ranged from 65 to 575 spikes/sec, with a population mean of 260 ± 124 spikes/sec (mean $\pm$ SD). These values are in agreement with previously reported results for P-type afferents in this species (Xu et al., 1996).

Interspike interval analysis

The discrete time interspike interval histogram for a representative spike train is shown in Figure 1*C*. For this unit, ISIs range from 1 to 7 EOD cycles ($\bar{I}_1 = 2.9$ EOD periods; $CV_1(1) = 0.47$). Mean ISIs of afferents ranged from 1.4 to 14.2 EOD cycles with a population mean of 4.2 ± 2.3 EOD cycles (Fig. 2*A*). The coefficient of variation of the ISI distribution ranged from 0.15 to 0.79 with a population mean of 0.44 ± 0.16 (Fig. 2*B*). Thus, on average, the SD of the ISI is ~44% of the mean, which reflects a considerable degree of variability in the baseline ISI distribution.

A representative joint interval histogram, which provides information about dependencies between adjacent intervals is shown in Figure 1*D*. Long intervals were more likely to be followed by short
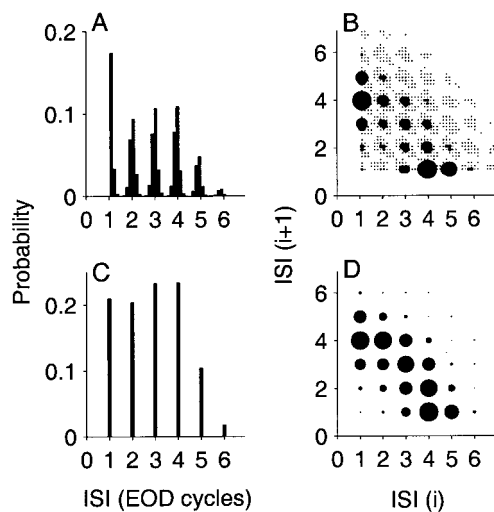
Figure 1. Interval histograms of a P-type primary afferent fiber from the weakly electric fish *Apteronotus leptorhynchus* showing continuous-time (*A*, *B*) and discrete-time (*C*, *D*) representations. *A*, ISI histogram. Abscissa is multiples of EOD period (EOD frequency, f = 762 Hz). *B*, Joint distribution of adjacent intervals (joint interval histogram). Abscissa and ordinate are the ith and $(i + 1)$th ISIs in EOD periods, respectively, with symbol sizes proportional to probability of occurrence. Bin width is 180 μsec in *A* and *B*. Resampling the spike train at the EOD rate restricts the interspike intervals to integer values as shown in *C* (ISI histogram) and *D* (joint interval histogram). This afferent had a mean ISI of 2.9 EOD cycles and coefficient of variation ($CV_I(1)$) of 0.47. Subsequent analysis in this paper is restricted to the discrete-time representation, in which spike trains are sampled at the EOD rate.

intervals and vice versa. Almost all fibers demonstrated a similar pattern.

The first-order ISI provides a characterization of spike time variability only on time scales comparable to the mean interspike interval. To characterize spike variability over longer time scales, the statistical properties of the higher-order interval distributions I_k must be considered. In particular it is informative to examine how the SD ($\sigma_I(k)$), coefficient of variation $CV_I(k)$, and the variance-to-mean ratio $F_I(k)$ vary as a function of interval order k. These are shown in Figures 3*A*–*C* respectively, for a representative afferent fiber ($\bigcirc$, *solid line*). The σ_I measured in EOD periods (Fig. 3*A*) grows slowly as k increases from 1 to ~60. Thereafter it increases rapidly (note logarithmic coordinates). Given that the mean of I_k obeys $\bar{I}_k = k\bar{I}_1$, i.e., it grows linearly with k, the initial slow growth in σ_I results in a decrease in the coefficient of variation $CV_I(k)$ (Fig. 3*B*) from an initial value of 0.58 (k = 1) until it reaches a plateau level of ~0.007 for interval orders $k > 100$. Thus, for high-order intervals, the SD is ~0.7% of the mean. This represents a reduction in CV_I on long-time scales by a factor of ~80 relative to the CV_I for the ISI. Similarly, for this unit, the variance-to-mean ratio $F_I(k)$ drops rapidly with increasing k from an initial value of 0.69 and reaches a minimum value of 0.02 for k = 59. Thereafter, F_I increases steadily for larger k. Both the minima in the F_I curve and the knee in the CV_I curve are a consequence of the transition
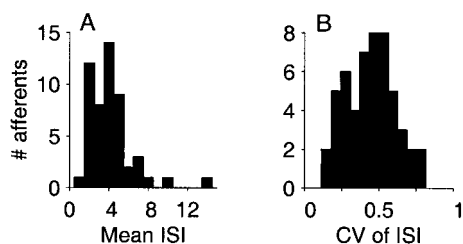
Figure 2. Population summaries of ISI distributions (N = 52). *A*, Distribution of mean ISI ($\bar{I}_1$). Abscissa is EOD cycles. *B*, Coefficient of variation of ISI ($CV_I(1)$).

in the behavior of σ_I from slowly varying to rapidly increasing (Fig. 3*A*).

The trends observed in σ_I, CV_I and F_I for this representative unit were consistent across the entire population. Figure 3*D*–*F* illustrates the population distribution for all 52 fibers by plotting the median value ($\bigcirc$, *thick line*) bracketed by the upper and lower quartiles (*thin lines*). For each fiber, we also determined the interval order k_{min}, which gave rise to the minimum variance-to-mean ratio F_I (Fig. 3*C*). The k_{min} were distributed across the population as shown in the gray histogram (Fig. 3*F*). The k_{min} for the population had a mean value of 42 ± 35. When these values are converted to EOD periods ($\bar{I}_1 k_{min}$) or milliseconds ($\bar{I}_1 k_{min} 10^{-3}/f$), they correspond to a mean time of 152 ± 121 EOD periods (or 176 ± 141 msec). The population means for the various measures at k_{min} were: σ_I, 2.9 ± 1.4 EOD periods; CV_I, 0.03 ± 0.02; and F_I, 0.08 ± 0.07 EOD periods. For 24 of 52 fibers, the SD was <2% of the mean interval length at k_{min} (Fig. 4*A*). This should be contrasted with the SD of the ISI where the mean $CV_I(1)$ for the population was 44% of the mean ISI (Fig. 2*B*).

The higher-order interval measures suggest that there may be two different regimes in time demarcated by k_{min}. When $k < k_{min}$, σ_I grows very slowly, and hence, both CV_I and F_I decrease as k^{-1}. That is, the interval distribution becomes less variable as k increases. When $k > k_{min}$, σ_I grows in proportion to k, and this causes CV_I to plateau and F_I to increase as k. In this regime, variability increases with increasing k. To analyze and interpret these results, interval statistics for afferents were compared with surrogate spike trains B, M_0, and M_1 described earlier.

Comparison with renewal process models

Binomial model

For each afferent fiber, a binomial model B was constructed from the p (per-cycle probability of firing) value of the fiber. Under baseline conditions p is a constant and is independent of firing activity in preceding EOD cycles. This model follows from a description of P units as probability coders (see Materials and Methods). The mean p for the population of fibers was 0.31 ± 0.14 and agrees with previously published results (Xu et al., 1996).

ISI and joint interval distributions for a representative fiber are shown in Figure 5, *A1* and *A2* (same data as in Fig. 1*C,D*). The corresponding distributions for a binomial model with the same p value are shown in Figure 5, *B1* and *B2*. Although the binomial model has the same p value, and thus the same mean ISI $\bar{I}_1 = 1/p$, it does not match the ISI or joint interval distributions of the data.

Nevertheless, the binomial model serves as a useful benchmark because the coefficient of variation CV_I and variance-to-mean ratio F_I can be computed analytically (see Appendix B). For the kth-order interval distribution, $\sigma_I(k) = \sqrt{k(1 - p)}/p$, $CV_I(k) = \sqrt{(1 - p)/k}$, and $F_I(k) = (1 - p)/p$ = constant. Spike trains generated from this model were subject to the same analysis as the data. These are shown in Figure 3*A*–*C* ($\square$, *dotted line*). Because $\sigma_I(k) \propto k^{1/2}$, in logarithmic coordinates, $\sigma_I(k)$ grows linearly with interval order k with a slope of 1/2 (Fig. 3*A*). It can be seen that the afferent has a much slower increase in σ_I for $k < 60$, but a much faster increase for orders >60. $CV_I(k)$ for the afferent data decreases more rapidly with increasing k (nearly as k^{-1}) than the binomial model for which $CV_I(k) \propto k^{-1/2}$ (Fig. 3*B*, $\square$) but eventually reaches a plateau for large interval orders. The distinction between the binomial model and the afferent data is most strikingly illustrated by the plot of the variance-to-mean ratio $F_I(k)$ shown in Figure 3*C*. For the binomial model $F_I(k)$ = constant, but the afferent data shows a strong dependence on interval order, initially dropping rapidly (nearly as k^{-1}) and reaching a minimum value for an interval order near 60. The population medians of σ_I, CV_I, and F_I for a binomial process with mean p obtained by averaging over all afferents are also shown in Figure 3*D*–*F* for comparison.

For each afferent fiber, we also determined the ratio of the $F_I(k_{min})$ for surrogate divided by afferent. Because the means of I_k are the same for afferent and the surrogate data sets (by construction), the above ratio is also the ratio of the variances of afferent
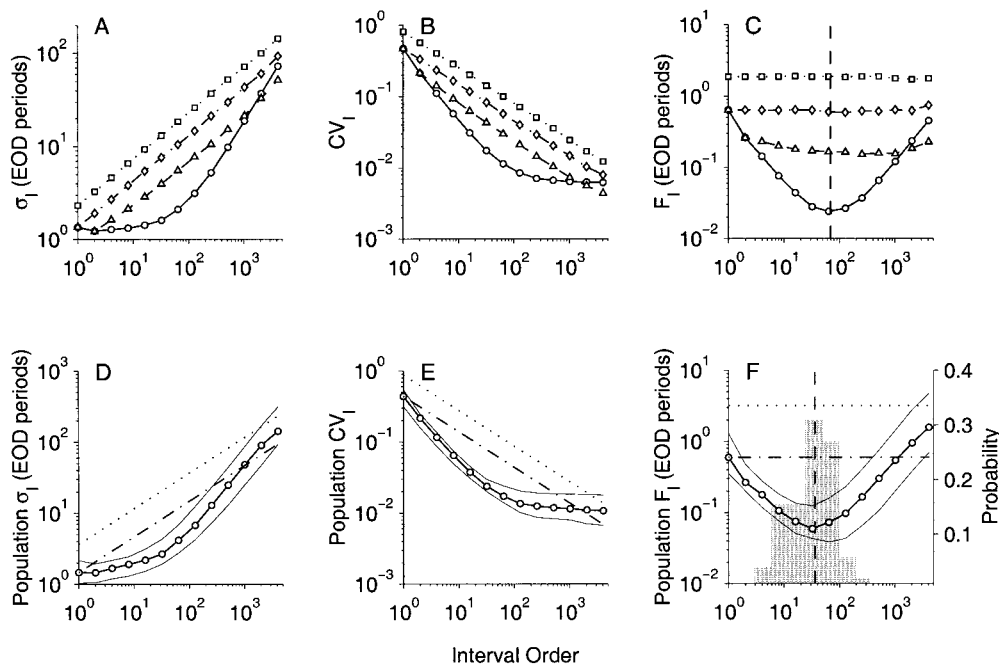
Figure 3. SD (σ_I, *left*), coefficient of variation (CV_I, *middle*), and variance-to-mean ratio (F_I, *right*) of interval distributions. *A–C*, Representative fiber shown in Figure 1; *D–F*, medians of population ($N = 52$). Abscissa is the interval order. Symbols are: afferent data (○) and surrogate data sets from binomial *B* (□), zeroth-order Markov M_0 (◇), and first-order Markov M_1 (△) processes. In *C*, the afferent F_I curve exhibits a minimum for interval order $k_{min} = 69$ (*vertical dashed line*). In *D–F*, the afferent data (○) are medians for the population ($N = 52$) and the *thin lines* are upper and lower quartiles. Also shown are renewal processes (binomial, *dotted*; zeroth-order Markov, *dash-dot*). The histogram in *F* represents distribution of k_{min} in the afferent population (probability on right axis), with mean value of 42 (*vertical dashed line*).
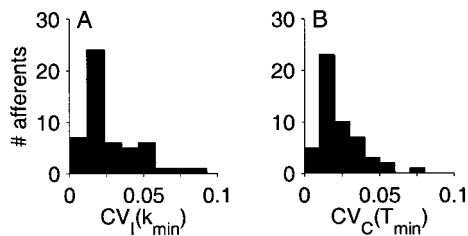
Figure 4. Population summaries of coefficient of variation evaluated at the minimum in the variance-to-mean ratio curve. *A*, CV_I for intervals at order $k = k_{min}$. *B*, CV_C for spike counts at count window length $T = T_{min}$ (see later in Results).

and binomial model at $k = k_{min}$. This ratio provides a measure of how much more regular the afferents are in comparison with the binomial process. Figure 6*A* shows the distribution of this number for the population. At $k = k_{min}$ the afferents exhibited variance-to-mean ratios that were on the average 50 times smaller (mean, 50 ± 27) than the F_I for binomial spike trains.

Zeroth-order Markov model (shuffled ISI)

The binomial model agrees with the data only in the mean value of the ISI distribution, but it fails to accurately describe the ISI distribution. The zeroth-order Markov model (M_0) was constructed for each afferent by shuffling the ISI sequence S_1 for that unit (see Materials and Methods). Thus, it matches the ISI distribution of the afferents. Figure 5, *C1* and *C2*, shows the ISI and joint interval distributions for this model. It can be seen that the model matches the ISI of the afferent (Fig. 5, compare *C1, A1*), however it does not correctly model the joint interval distribution (Fig. 5, compare *C2, A2*).

Because M_0 is a renewal process, the coefficient of variation CV_I and variance-to-mean ratio F_I can be computed analytically (see Appendix B): $CV_I(k) = CV_I(1)/\sqrt{k}$, where $CV_I(k) = \text{Var}(I_1)^{1/2}/\bar{I}_1$, and $F_I(k) = \text{Var}(I_1)/\bar{I}_1 = $ constant. Results for this model matched to a representative afferent are shown in Figure 3*A–C* (◇, *dash–dot*

line). Note that $\sigma_I(1)$, $CV_I(1)$, and $F_I(1)$ (i.e., the *y* intercepts) are the same for M_0 and afferent because M_0 was constructed to match the first-order statistics of the data. The population σ_I, CV_I, and F_I curves for this model are shown in Figures 3*D–F*, respectively (*dash–dot line*).

Although M_0 is more regular than the binomial model *B*, it still does not capture the intermediate-term regularity of the afferent data. At the minimum of the variance-to-mean ratio curve, F_I for the data was on average 14 times smaller (mean, 13.8 ± 10.1) than for M_0 (Fig. 6*B*). Whereas this is an improvement over the binomial model, the reduction in variability with increasing order of intervals is not as great as that demonstrated by afferents.

The above results show that variability in afferent interval distributions cannot be accounted for by an underlying renewal process. In particular, at the minima in the F_I curve, which occurs on a time scale of ~60 intervals (~200 msec), afferents have a variance that is an order of magnitude smaller than that predicted by a renewal process. Thus, we must look at nonrenewal properties for a better understanding of this dramatic reduction in spike train variability.

Comparison with nonrenewal models

Renewal models are "memoryless", that is interval distributions are independent of previous intervals. However, this is not the case for P-type afferent data, as illustrated by the joint interval distribution (Fig. 5*A2*). Long intervals in the sequence are more likely to be followed by short intervals and vice versa. In contrast, neither of the renewal models (B, M_0) discussed above incorporate this dependency, as can be seen from Figure 5, *B2* and *C2*.

The simplest nonrenewal model that incorporates the observed long–short dependency is the first-order Markov process M_1 described earlier (see Materials and Methods) where the probability of generating the next interval depends only on the current interval. Figure 5*D2* shows the joint interval histogram for the fiber shown in Figure 5*A2*. By construction, the ISI distribution $I_1(j_1)$ (Fig. 5*D1*), joint interval distribution $I(j_1, j_2)$ (Fig. 5*D2*), and second-order interval $I_2(j_1)$ distribution (data not shown) are identical to those of the afferent.
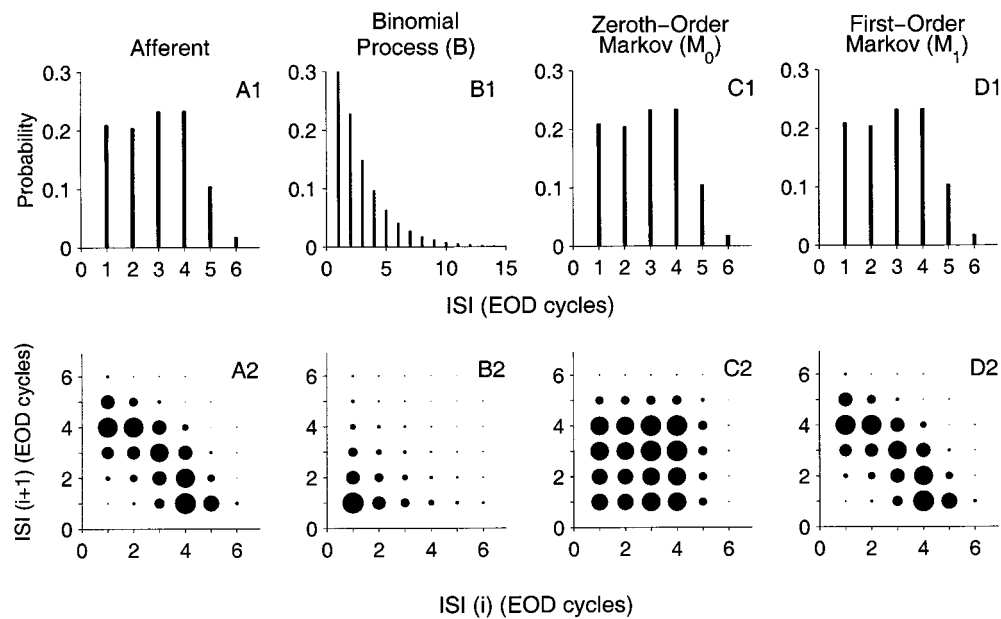
Figure 5. ISI histogram and joint interval histogram of the afferent spike train shown in Figure 1 (column *A*) and surrogate spike trains obtained from the afferent data (columns *B–D*). *A1–D1*, Show the first-order ISI histograms $I_1(j)$, and *A2–D2* show the joint interval histogram $I(j_1, j_2)$ of adjacent ISIs. *Size* of the *circle* is proportional to joint probability. *B*, The binomial spike train matches the mean ISI $\bar{I}_1$, but it does not match either the ISI or joint ISI distributions. *C*, The zeroth-order Markov spike train (M_0) matches only ISI, but not the joint interval distribution. *D*, The first-order Markov spike train (M_1) matches both the ISI and joint ISI of the afferent spike train. ISI sequences for *B* and M_0 are renewal processes, whereas M_1 is a nonrenewal process.
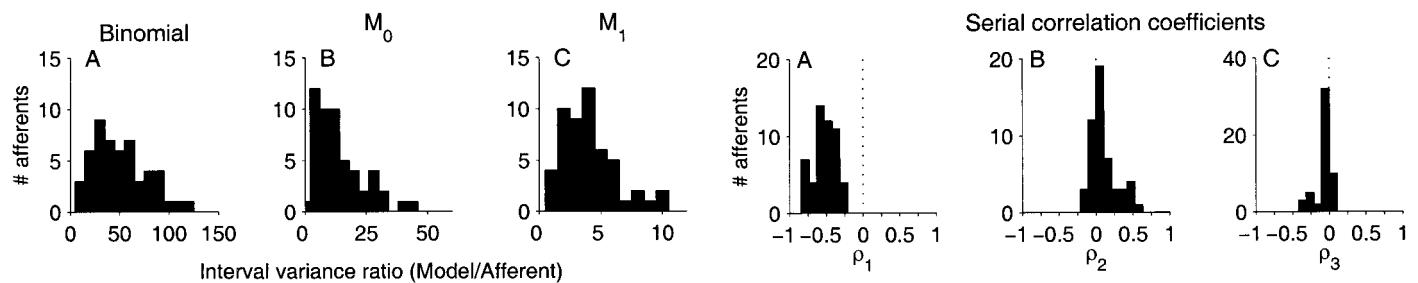
Figure 6. Population summaries of the decrease in interval variance-to-mean ratio (F_I) observed in afferents when compared to F_I of the matched surrogate spike trains: *A*, binomial, *B*, zeroth-order Markov (M_0), and *C*, first-order Markov (M_1). Each histogram is the distribution of the ratio of the $F_I(k_{min})$ for surrogate divided by afferent. It measures the decrease in variability of intervals in afferents with reference to the surrogate spike train. Note different scales on abscissa.

Figure 7. Population summaries of serial correlation coefficients (ρ) of afferent ISI sequences. *A–C*, First three lags, ρ_1–ρ_3, respectively. The *vertical dashed line* is $\rho = 0$. The negative correlation for adjacent ISIs (ρ_1) reflects the strong long–short dependency in the ISI sequence.

Results for the M_1 model are shown in Figure 3*A–C* ($\triangle$, *dashed line*). σ_I, CV_I, and F_I are identical for M_1 and afferent for $k = 1$ and $k = 2$ (by construction), but thereafter, M_1 does not fully capture the continued decrease in variability observed in the afferent data, although it is better than the two renewal models B and M_0.

At the minimum order k_{min}, F_I for the afferents was on average a factor of four times smaller than the M_1 model (mean, 4 ± 2) (Fig. 6*C*). Thus, even a nonrenewal model that correctly incorporates the long–short correlations exhibited in the data cannot adequately account for the longer term regularity of afferent spike trains. This result indicates that dependencies in the underlying nonrenewal process go beyond the immediately preceding ISI. The analyses in the following sections are intended to address how far back in time the "memory" effect extends.

Interval correlations

Correlations over longer durations were analyzed for each afferent and its matched M_1 model using serial correlation coefficients (Eq. 7). Figure 7*A* shows the population distribution of the correlation coefficient between adjacent ISIs (ρ_1). The ρ_1 ranged from -0.23 to -0.82 with a population mean of -0.52 ± 0.14. That is, all afferents exhibited strong long–short ISI dependency. The distri-

bution of correlation coefficients in the population for lags of 2 and 3 are shown in Figure 7, *B* and *C*. Most afferents exhibit positive correlations for lag = 2 ($\bar{\rho}_2$, 0.10 ± 0.18) and weak negative correlations for lag = 3 ($\bar{\rho}_3$, -0.07 ± 0.11). However, for lags larger than one, the coefficients become smaller, and we used more rigorous statistical criteria to determine the extent and significance of the ρ_k.

Serial correlation coefficients were estimated for all fibers for the first 10 lags. Coefficients are shown for three representative fibers in Figure 8 (*solid line*), and the first-order Markov model M_1 (*dash-dot line*). Spike trains from the renewal models B and M_0 did not exhibit any correlations (i.e., $\rho_k = 0$, for all k) because of independence of ISIs (data not shown). For both afferent and model M_1 we used a shuffled data technique to determine the maximum lag k for which the ρ_k were significantly different from zero (see Materials and Methods).

Although all fibers exhibited statistically significant correlations extending back several lags, so did the M_1 model. In fact, in almost all cases, the M_1 model showed much stronger correlations than the afferent for all lags $k \geq 2$. Thus, even a Markov process that is first-order (M_1) can have nonzero SCCs that extend much further back in time than a single interval.

The following example illustrates the converse effect that the SCC for lag l can be small even when there are strong lth order dependencies in the data. To illustrate this point we took the ISI
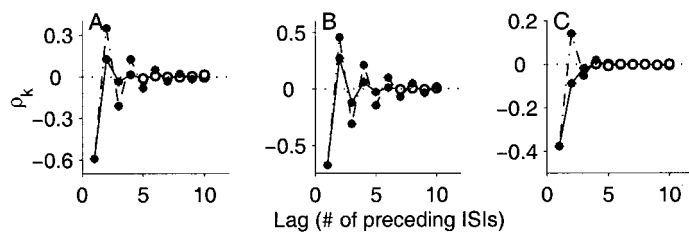
Figure 8. Representative serial correlation coefficients (ρ_k, ordinate) for lags $k = 1, \ldots, 10$ (abscissa). The ρ_k measure correlation between an ISI and the kth preceding ISI. *A–C* show ρ_k for three representative afferents (*solid line*) and for their matched surrogate first-order Markov spike train M_1 (*dash-dot line*). Coefficients were tested against the null hypothesis that there was no correlation between the intervals at $p = 0.01$. The ρ_k which are significantly different from zero are indicated by *, whereas ○ indicates no significant correlation.
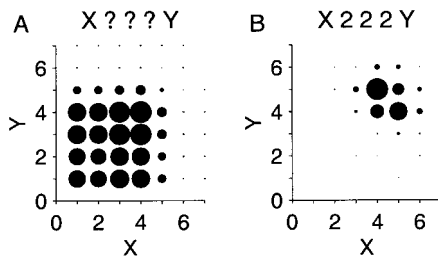

Figure 9. An illustration of how correlation analysis may fail to reveal memory effects in spike trains. *A*, Patterns of four adjacent ISIs (*X*, ?, ?, ?, *Y*) where "?" is any arbitrary value, were extracted from the ISI sequence S_1 for the afferent shown in Figure 1. The joint probability distribution of *X* and *Y* were estimated (probability is proportional to diameter of the *circle*). The joint distribution suggests a very weak correlation between *X* and *Y* (see Results). *B*, Patterns of four adjacent ISIs (*X*, 2, 2, 2, *Y*) were extracted as in *A*. The distribution of *X* and *Y* is strongly influenced by conditioning it on the intermediate sequence (2, 2, 2). Serial correlation coefficients provide information from the distribution shown in *A* and not from the conditioned distribution shown in *B*. Hence, long-term memory effects may not be noticeable from correlation analysis.

sequence S_1 for the representative afferent illustrated in Figure 1 and analyzed the distribution of $Y = S_1(i)$, given $X = S_1(i - 4)$ for two example patterns: (*X*, ?, ?, ?, *Y*) and (*X*, 2, 2, 2, *Y*). In the first pattern the "?" represents any arbitrary ISI, i.e., *X* and *Y* were not conditioned on the intervening intervals ($S_1(i - 3)$, $S_1(i - 2)$, $S_1(i - 1)$). However, in the second sequence, *X* and *Y* were conditioned on the occurrence of a specific sequence ($S_1(i - 3) = 2$, $S_1(i - 2) = 2$, $S_1(i - 1) = 2$). We then calculated the joint probability of *Y* given *X* as for Figure 1*D* (see Materials and Methods). The results are shown in Figure 9.

Figure 9*A* shows that *X* and *Y* are only weakly correlated ($\rho_4 = 0.014$; $p = 0.01$). It is useful to compare this histogram with that of the zeroth-order Markov process for the same afferent as shown in Figure 5*C2*. The zeroth-order model is a renewal process where intervals are uncorrelated for all lags *k*. The similarity between the two histograms suggests a loss of correlation. In contrast, the pattern (*X*, 2, 2, 2, *Y*) has a joint distribution shown in Figure 9*B*, and it can be seen that conditioning very strongly influences the correlation structure of the joint distribution. Because serial correlation analysis is based on unconditioned distributions, long-term memory effects may average out.

Analysis of Markov order

The above examples illustrate the shortcomings of serial correlation analysis of memory effects and indicate that a more direct test of Markov order is needed. Toward this end we applied a statistical test to explicitly test the Markov order of the process (see Materials and Methods). Each afferent was tested against surrogate data sets that were constrained to match the afferent up to a specified order *m*. The test statistic was the conditional entropy h_{m+1}. Testing
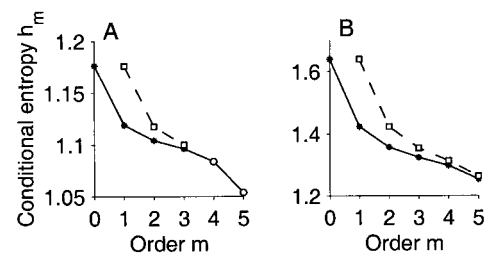
Figure 10. Conditional entropy h_m for two representative afferent spike trains (*solid line*) as a function of order *m*. The mean h_m for 49 surrogate sequences which matched the data exactly up to order ($m - 1$) are also shown (□, *dash line*). Afferent h_m, which were significantly different from surrogate data are shown as *. Differences between afferent and surrogate data which were not significant are shown as ○. *A*, Afferent spike train that was described by a third-order Markov process. *B*, Spike train for which surrogate and afferent data sets had significantly different h_m for all orders tested. Testing terminated because of insufficient data. The order of the process was at least 5, i.e., the number represents only a lower-bound. See Table 1 for a summary of testing.

began with $m = 0$ and continued for increasing values of *m* until the null hypothesis (process is of order *m*) could not be rejected.

Results for two representative afferents are shown in Figure 10, which depicts the h_m for afferent (*solid line*) and mean h_m for 49 realizations of the surrogate data (*dashed line*). For the unit shown in Figure 10*A*, testing showed that afferent data had significantly smaller h_m(*) than surrogate data (□) for orders up to 3. For orders 4 and 5, there was no significant difference in the h_m (○). It was concluded that this afferent could be described by a third-order Markov process. Testing terminated for only 5 of 52 afferents with the null hypothesis being accepted. Testing also terminated if there was not sufficient data for the afferent. This is shown in Figure 10*B*, where the afferent and surrogate data sets were significantly different up to fifth-order. There was not sufficient data to test for higher orders, and thus $m = 5$ is only a lower-bound on the order of the process for this afferent. Testing terminated for the majority of afferents (47 of 52) in this way.

Table 1 summarizes the test for Markov order. The total number of afferents for which the order was at least *m* are listed for each *m* in the top row. Of these, the number of afferents for which the order was exactly *m* are shown in the bottom row. For example, all 52 afferents were at least order 2 (top row, $m = 1, 2$), with one afferent being exactly order 2 (bottom row, $m = 2$). Similarly, 51 were at least order 3, of which three afferents were exactly order 3. Thus, discarding the three afferents that were exactly order 3, only 48 afferents were tested for $m = 4$. Four of these could not be tested because of insufficient data, leaving 44 afferents that were at least order 4 (top row, $m = 4$). Of these afferents, only one was exactly order 4 (bottom row, $m = 4$). The test proceeded in this manner until afferents were exhausted. Most afferents (44 of 52) were fourth-order Markov or greater, and approximately a quarter of the units (12 of 52) were seventh-order Markov or greater.
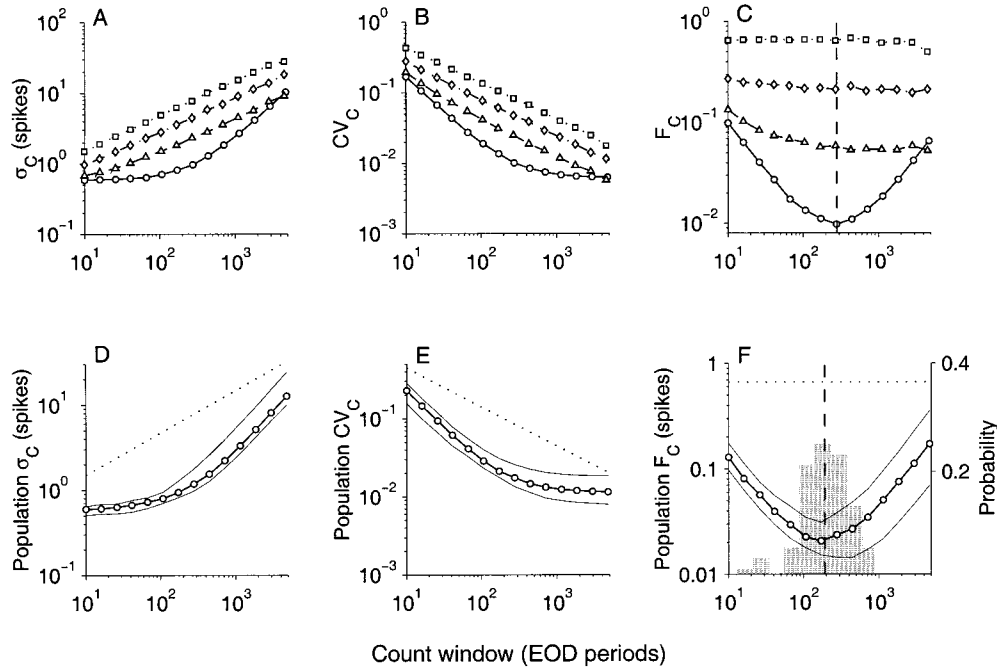
Count distributions

For nonrenewal processes, spike count distributions can provide additional information about the process and can complement higher-order interval analysis. Spike count distributions were analyzed from the count sequence defined by Equation 2. The SD σ_C, coefficient of variation CV_C, and variance-to-mean ratio F_C (also called Fano factor) of the spike count distributions were computed as a function of window duration *T*. *T* plays the same role in count analysis as interval order *k* in interval analysis.

Figure 11*A–C* shows the statistical measures for the same representative afferent fiber, whose interval analysis was described earlier (Fig. 3*A–C*). As with interval analysis, spike count distributions exhibited a minimum variance-to-mean ratio (Fano factor F_C) at an optimum count window of duration T_{min}. For the fiber shown in Figure 11*C*, $T_{min} = 280$ EOD periods (368 msec) with

Table 1. Test of Markov order for N = 52 units

| Number of afferents	Markov order m											
	0	1	2	3	4	5	6	7	8	9	10	11
Order ≥ m	52	52	52	51	44	24	16	12	4	3	1	1
Order = m	0	0	1	3	1	0	0	0	0	0	0	0

Each unit was tested under the null hypothesis that it was generated by a Markov process of order m, where initially $m = 0$. If the unit failed the test then it was considered to have order ≥ m, and m was increased and the test performed again. For each order m (columns), the number of units that were at least order m are listed in the top row. As m increased, the number of units tested decreased either due to insufficient data or because a unit satisfied H_0 for some previous order (bottom row).

Figure 11. SD (σ_C, *left*), coefficient of variation (CV$_C$, *middle*), and variance-to-mean ratio (Fano factor F$_C$, *right*) of spike count distributions. *A–C*, Representative afferent (same afferent shown in Fig. 3*A–C*). *D–F*, Medians of population (N = 52). Abscissa is count window duration T in EOD cycles. Symbols and layout follow Figure 3. In *C*, afferent F$_C$ curve exhibits minima when count window T_{min} = 280 EOD periods (*vertical dashed line*). In *D–F* the *dotted line* is the median for surrogate binomial data with mean ISI equal to that of the afferent population. The histogram in *F* is the distribution of T_{min} in the afferent population, with mean value T_{min} = 233 EOD periods (*vertical dashed line*).

F$_C$(T_{min}) = 0.01 spikes. Mean spike count at T_{min} was 94 ± 0.98 spikes, i.e., a SD that is ~1% of the mean (Fig. 11*A,B*). Beyond this minimum T, counts became more irregular with increasing T because of the rapid increase in SD (Fig. 11*A*). The trends in σ_C, CV$_C$, and F$_C$ were observed in all afferents and closely resemble those seen in interval analysis (Fig. 3). Figure 11*D–F* summarizes the median value of σ_C, CV$_C$, and F$_C$ for the population. The distribution of T_{min} across the population is shown in the histogram overlaying the Fano curves in Figure 11*F*. Mean T_{min} for the population was 233 ± 172 EOD periods (270 ± 200 msec), and mean F$_C$(T_{min}) for the population was 0.025 ± 0.022. At T_{min} when fibers demonstrate most regular counts, the distribution of CV$_C$(T_{min}) for the population is shown in Figure 4*B*. Twenty seven of 52 fibers had SDs that were <2% of mean spike count. Mean CV$_C$(T_{min}) for the population was 0.026 ± 0.023.

As was the case for interval analysis, the spike count analysis indicates that the afferents are significantly more regular than the three model spike trains (*B*, M_0, and M_1). The improvement in regularity measured as a ratio of the Fano factor of the model to that of the afferent at T_{min} is shown in Figure 12. The figure is similar to Figure 6. Afferents had Fano factors that were on the average smaller than those of the models by 19.6 ± 10.5 (*B*, Fig. 12*A*), 6.0 ± 4.7 (M_0, Fig. 12*B*), and 1.7 ± 1.0 (M_1, Fig. 12*C*). Thus, the count analysis agrees with interval analysis in that the regularity of afferents cannot be explained by renewal models (*B* and M_0) or even a nonrenewal model that incorporates adjacent interval dependencies (M_1).
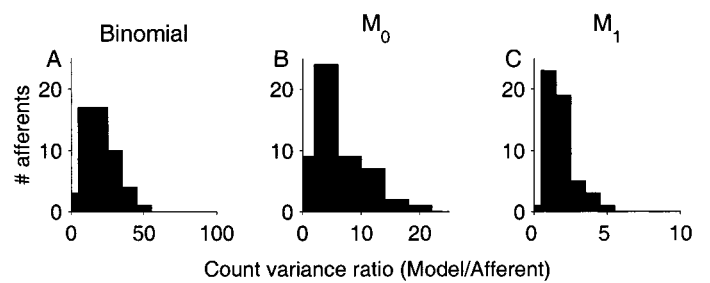
Figure 12. Population summaries of the decrease in count variance-to-mean ratio (Fano factor, F$_C$) observed in afferents when compared to F$_C$ of the matched surrogate spike trains: *A*, binomial; *B*, zeroth-order Markov (M_0); and *C*, first-order Markov (M_1). Each histogram is the distribution of the ratio of the F$_C$(T_{min}) for surrogate divided by afferent. It measures the decrease in spike count variability in the afferents with reference to the surrogate spike trains. Note different scales on abscissa.

Although interval and count analysis are in agreement on the general trends seen in afferent data, it should be noted that there are differences between the two. The most significant difference lies in a determination of the time scale on which afferents may be considered most regular. From interval analysis, the mean time estimated for the population at their k_{min} was 176 msec (see Interspike interval analysis), which is smaller than the mean T_{min} estimated at 270 msec from the count analysis (see above).
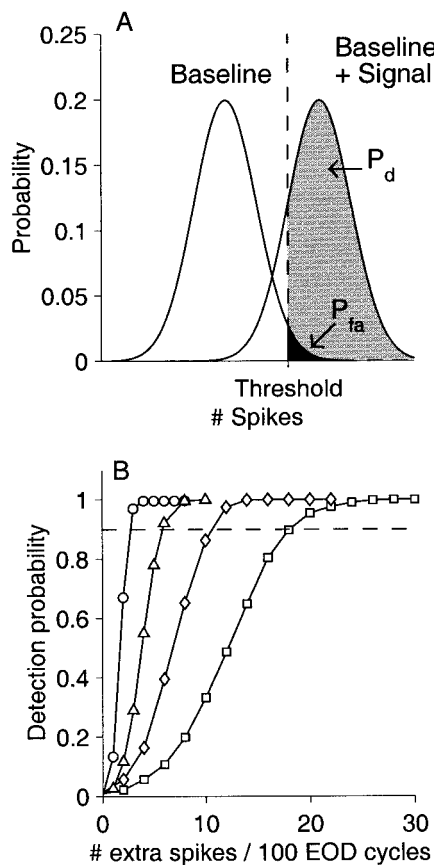
Figure 13. Signal detectability in afferent spike trains when spikes are added at random to baseline discharge. *A,* The detection strategy is based on a binary hypothesis test. In the presence of a signal, the baseline spike count distribution (*Baseline*) is shifted by an amount equal to the increase in number of spikes caused by signal (*Baseline + Signal*). A threshold (*vertical dashed line*) defines the probability of detection (*gray area, P_d*) and probability of false alarm (*black area, P_{fa}*). By constraining P_{fa}, P_d can be maximized. *B,* Spikes (abscissa) were added randomly to blocks of $T = 100$ EOD periods, and a signal detection algorithm (see Results) was given the task of determining whether signal was present subject to $P_{fa} \leq 0.001$. Ordinate is P_d, and abscissa is number of extra spikes caused by signal. Detection experiments were simulated in afferent ($\bigcirc$), and surrogate spike trains from binomial (B, $\square$), zeroth-order Markov (M_0, $\diamond$), and first order Markov (M_1, $\triangle$) processes. For the afferent, signal detection performance at 90% (*dashed line*) is possible with as few as 2–3 spikes over the baseline of 35 spikes. Surrogate spike trains required more spikes to achieve the same level of performance (see Results).

Weak signal detection

The regularity of primary electrosensory afferent spike trains is most pronounced for count windows on the order of ~200 EOD periods (~200 msec). Here, we illustrate the impact that this spike count regularity could have on detection performance, if the nervous system were to implement a detection algorithm using a comparable integration time constant. Full analysis of the optimal detection algorithm for the actual spatiotemporal profiles of naturally occurring electrosensory signals is beyond the scope of this paper. Here, we demonstrate the magnitude of the effect by considering a simplified signal detection experiment in which the stimulus is assumed to transiently increase the spike count on an individual afferent by a fixed number of spikes n_s within a fixed time window.

The detection algorithm is based on an ideal observer paradigm (Green and Swets, 1966) using spike count distributions (see Materials and Methods). It implements a binary hypothesis testing procedure illustrated schematically in Figure 13*A*. In the absence of a stimulus, the spike count is drawn randomly from the baseline spike count distribution (Fig. 13*A, Baseline*). In the presence of the stimulus, the spike count is assumed to be drawn from a shifted

version of the same distribution, with an offset of n_s spikes (Fig. 13*A, Baseline + Signal*). Given an observed spike count, the detection experiment decides which of the two distributions is most likely to have generated the observation. If the count exceeds a fixed threshold (Fig. 13*A, Threshold*), then we decide that a stimulus event has occurred. This could be a false alarm because of a baseline fluctuation being erroneously classified as a stimulus event (area marked as P_{fa} under the *Baseline* curve) or a correct detection if a stimulus was in fact present (area marked as P_d under the *Baseline + Signal* curve).

Simulated signal detection experiments were performed using afferent data from a representative unit, as well as three matched spike train models (B, M_0, and M_1). The results are shown in Figure 13*B*. In all cases the detection probability P_d increased with increasing signal strength n_s, but it increased more rapidly with increasing number of added spikes for the afferent than for any of the three models. If we arbitrarily select $P_d = 0.90$ for comparison purposes (Fig. 13*B, horizontal dashed line*), we find that an addition of two or three spikes results in a 90% detection probability for the afferent spike train, whereas a comparable level of performance requires approximately five spikes for M_1, 10 spikes for M_0, and 18 spikes for the binomial process B. Specifically, comparing results for the afferent data and the best-matched renewal process model M_0, we see that the afferent spike train permits efficient and reliable detection of signals that are a factor of 3–5 times weaker than could be detected if baseline activity were generated by a renewal process.

DISCUSSION

The principal finding of this study is the remarkable regularity of P-type afferents on intermediate time scales, given the high variability of their interspike intervals on short time scales. We measured variability of intervals using SD (σ_I), coefficient of variation (CV_I), and variance-to-mean ratio (F_I). Across the population of afferents the coefficient of variation of the first-order ISI, $CV_I(1)$, averaged ~0.44. Higher-order intervals I_k (which are the sums of k successive ISIs) showed a rapid decrease in CV_I. On intermediate time scales ($k \approx 50$), $CV_I(k)$ was <0.02 for most afferents (Fig. 3*E*). In contrast if the intervals were generated by a renewal process, CV_I would decrease as $k^{-1/2}$, and the expected CV_I on intermediate time scale would have been ~3–5 times larger.

Although CV_I is a normalized measure of variability, it is easier to understand the large improvements in regularity of afferents by examining how the standard deviation of intervals σ_I changes with k (Fig. 3*A*). For a renewal process σ_I increases as $k^{1/2}$, but for afferents, there is little increase in σ_I up to $k \approx 50$ (Fig. 3*A*). It is as if the spike-generating process were keeping a check on the cumulative deviation of the successive ISIs from the mean ISI. Such a regularizing process could cancel deviations so that overall variability of k successive intervals is approximately the same as the variability of a single interval. If such a process were responsible for the observed regularity it would appear that the process is able to maintain this regularity only over intermediate time scales. This is seen most clearly in the variance-to-mean ratio curve F_I (Fig. 3*C*). The F_I curve decreases sharply with increasing k, whereas a renewal process has constant F_I. For the afferent data, F_I decreases until it reaches a minimum (for some afferent specific k_{min}), after which it loses regularity and increases with increasing k. The time scale on which the spike regularity is most pronounced relative to a renewal process corresponds to interval order k_{min}. The distribution of k_{min} in the population of afferents is shown in the *gray histogram* of Figure 3*F*. The population mean was $\bar{k}_{min} = 42$, which corresponds to ~175 msec. Spike count distributions (Fig. 11) demonstrated similar trends, although the estimated time scale over which spike counts were most regular was somewhat larger (270 msec).

The rapid decrease in variability has implications for signal detection. For a renewal process, to achieve a similar reduction in variability would require a time scale of about k_{min}^2, which is ~1700 ISIs, or several seconds. Therefore, in situations where sensory

signals are extremely weak, the regularization process allows reliable detection using smaller integration times.

Interval and count variability in other sensory systems

The coefficient of variation of the ISI distribution has long been the standard measure for specifying spike train variability. For the benchmark Poisson process, $CV_I = 1$ for all interval orders. Spike trains with $CV_I > 1$ (< 1) are more irregular (regular) than a Poisson process. Spontaneously active neurons demonstrate a wide range in ISI variability with reported values ranging over two orders of magnitude from 0.02 (Ratliff et al., 1968) to ~3 (Teich et al., 1997). In comparison, the values we report here for P-type electroreceptor afferents had a mean $CV_I(1)$ of 0.44 and ranged from 0.15 to 0.79, reflecting moderate to high short-term variability.

For renewal processes, the ISI distribution is sufficient to completely describe variability on all time scales (Cox, 1962). For nonrenewal spike trains, such as P-type afferents reported here, it is necessary to examine higher-order distributions. Towards this end, interval distributions I_k or count distributions C_T and their statistical properties can provide useful information about variability. Higher-order interspike interval distributions were first introduced by Rodieck et al. (1962), but with the exception of second-order interval distributions I_2 (Teich and Khanna, 1985) they have not been widely used. This is unfortunate because higher-order interval distributions convey useful information about variability on multiple time scales. On the other hand, spike count distributions have been more widely used in recent years. However, they have been used primarily to characterize spike trains for which the Fano factor exhibits power-law growth with count window T, on time scales extending beyond tens of seconds (for review, see Teich et al., 1996). Such spike trains exhibit a high degree of irregularity ($F_C > 1$) that increases with counting time. On the time scales that are of interest to us (0.1–1 sec), most of the reported work on spike count distributions are restricted to driven responses (Teich and Khanna, 1985; Young and Barta, 1986; Relkin and Pelli, 1987; Shofner and Dye, 1989; Softky and Koch, 1993; Baddeley et al., 1997; Shadlen and Newsome, 1998) and cannot be directly compared with the results for baseline responses.

History effects and nonrenewal nature of afferent spike trains

Most experimentally observed spike trains exhibit correlations and memory effects in the ISI sequence. That is, they are described by nonrenewal processes. This is true for all P-type afferents reported here. All afferents had adjacent ISIs that were strongly anticorrelated. Anticorrelations have been noted in spike trains of P-type units in other species of electric fish such as the gymnotid *Sternopygus* (Bullock and Chichibu, 1965) and *Steatogenes* (Hagiwara and Morita, 1963). They have also been reported in many other sensory systems including visual (Kuffler et al., 1957), auditory (Johnson et al., 1986; Lowen and Teich, 1992), and somatosensory (Amassian et al., 1964), and in motor systems (Calvin and Stevens, 1968). Whereas anticorrelation improves regularity, our results suggest that it is not sufficient to account for the dramatic improvements in regularity observed in P-type afferents. We demonstrated that a first-order Markov process M_1 that incorporated the anticorrelations observed in the afferent data could not reproduce the reduction in variability demonstrated by the afferent spike trains with increasing T (Fig. 11). This suggested that dependencies between ISIs persisted over many intervals.

To assess the duration of history-dependent effects, serial correlation coefficients were evaluated. However, SCCs suffer from two problems. First, even a first-order Markov process can have statistically significant correlations that persist over many intervals (Fig. 8). Second, even if a process is higher-order Markov (Fig. 9B), the use of serial correlation coefficients can average out effects of dependencies for lags smaller than the Markov order (Fig. 9A). Thus, Figures 8 and 9 demonstrate that the SCCs cannot be used to determine the order of the Markov chain, and an explicit test of Markov order is required (Nakahama et al., 1972). When explicitly

tested for the order of the underlying Markov chain, the majority of afferents were typically fourth-order or greater (as also reported by van der Heyden et al., 1998).

The high degree of regularity exhibited by afferents is a consequence of a nonrenewal process that keeps a check on the deviation from the mean firing rate over many ISIs. Typically, when an interval longer than the mean ISI occurs (a "credit"), the next interval will be shorter than the mean (a "debit"). This gives rise to the strong long–short anticorrelations observed in the data. However, when the credit does not get paid back immediately, it is not forgotten. Rather, it is paid back eventually. This is seen from Figure 9B where we evaluated the distribution of Y given the previous occurrence of X in the ISI sequence $(X, 2, 2, 2, Y)$. The joint distribution shows that the long–short distribution of intervals persists even when there are a number of intervening intervals where the debits and credits do not cancel each other. It is likely that the demands placed on a physiological system for maintaining precision or regularity of spiking may be more easily achieved by making adjustments in timing over many intervals rather than over a few intervals. At present the mechanism causing this remarkable degree of precision is unknown. Although mathematical models of the spike-generating process in P-type afferents have been constructed (Longtin and Racicot, 1997b; Longtin, 1998), they do not explain the long-range interval correlations noted here.

Implications for detection of weak sensory signals

The increased spike train regularity that we observe for P-type afferents on intermediate time scales has important implications for the ability of the fish to detect weak electrolocation targets. P-type afferents encode amplitude modulations of the local transdermal voltage caused by nearby objects (Scheich et al., 1973; Bastian, 1981) (for review, see Zakon, 1986). Objects in the water near the fish modulate the transdermal potential and thus modulate the per-cycle firing probability of P-type afferents. Objects that cause a large change in firing probability are easily detected by the animal. However, when the object is small, or far away, or has low electrical contrast with the surrounding water, then the resulting small change in per-cycle firing probability can be obscured by statistical fluctuations in the baseline spike activity. Early studies have established that the behavioral threshold for *Apteronotus* is <1 μV/cm (Knudsen, 1974). Bastian (1981) extrapolated his data to show that in this range, the change in firing rate of P-type afferents is ~1 spike/sec. Thus, at threshold levels of performance the expected change in firing rate is <1% (based on a mean discharge rate of 294 spikes/sec as reported by Bastian, 1981).

In behavioral studies of prey capture performed in our laboratory, we have shown that *Apteronotus* can detect small water fleas (*Daphnia magna*, 2–3 mm in length) at a distance of ~2 cm from the electroreceptor array (Nelson and MacIver, 1999). At this distance, the spatial profile of local transdermal voltage change is a Gaussian-like bump with a full width at half maximum of ~2 cm (Rasnow, 1996; Nelson and MacIver, 1999). During prey capture behavior the fish is typically moving with a relative velocity of ~10 cm/sec relative to the prey. Thus, as the electrosensory image passes over the receptor array, an individual electroreceptor organ experiences a transient change in transdermal voltage that lasts ~200 msec. Interestingly, this temporal duration is well matched to the time scale on which P-type afferents show the greatest increase in spike train regularity.

Based on computer reconstructions of electrosensory images from our behavioral studies, we estimate that the peak change in per-cycle firing probability of P-type afferents at the time of prey detection is at most a few percentage of the baseline probability (Nelson and MacIver, 1999). Assuming a typical baseline spike rate of 300 spikes/sec, this corresponds to approximately one extra spike of a total of 60 spikes expected in a 200 msec time window on an individual afferent. This is a weak signal and one that could potentially be difficult to detect given the relatively high variability observed in the first-order ISI distribution.

The neural computations required to detect the dynamically

changing spatiotemporal profile across a population of electrosensory afferents could plausibly be implemented by circuitry in the brainstem electrosensory nucleus, the electrosensory lateral line lobe (Shumway, 1989; Metzner et al., 1998). A full analysis of the optimal detection algorithm is beyond the scope of this paper. However, in performing such an analysis, it will be extremely important to take into account the intermediate-term regularity of P-type afferent spike trains afforded by the underlying nonrenewal process. If we performed such an analysis assuming that P-type afferents could be adequately modeled by matching the first-order ISI distribution and assuming a renewal process model, we would overestimate the behavioral threshold by a large factor (Fig. 13*B*). Thus, it is important for sensory physiologists and neural modelers to consider potential effects of nonrenewal statistics when analyzing detection thresholds for weak sensory signals in noisy spike trains.

APPENDIX A

Spike count distributions for discrete-time renewal processes

For spike trains arising from a discrete-time renewal process, the distribution of spike counts can be calculated from the distribution of interspike intervals. To illustrate this, we first present results for the binomial spike train and then derive expressions relating count and interval distributions for arbitrary renewal processes.

For a binomial process with constant per-cycle probability of firing p, the probability of observing an interval of j cycles between successive spikes is:

$$I_1(j) = p(1 - p)^{j-1}, \tag{10}$$

which is the geometric distribution with mean $\bar{I}_1 = 1/p$. In general, the probability of observing an interval j between k successive spikes (i.e., the kth order interval distribution) is:

$$I_k(j) = \begin{cases} \binom{j-1}{k-1} p^k (1-p)^{j-k} & j \ge k, \\ 0 & j < k, \end{cases} \tag{11}$$

with mean $\bar{I}_k = k/p$. Equations 10 and 11 are the discrete time analogs of the exponential and kth-order gamma distributions, respectively.

For a binomial process, the number of spikes in a count window of duration T cycles is distributed according to:

$$\hat{C}_T(k) = \binom{T}{k} p^k (1-p)^{T-k}, \tag{12}$$

where $\hat{C}_T(k)$ is the probability of finding k spikes in T cycles.

For an arbitrary discrete-time spike-generating process, if counting is performed so that the window starts on the cycle immediately after a spike, then the distribution for the number of spikes in a window of size T, $\hat{N}_T$, is related to the distribution of the kth order spike intervals, S_k, by:

$$\text{prob}\{\hat{N}_T < k\} = \text{prob}\{S_k > T\}, \, k \ge 1. \tag{13}$$

In other words, the probability that there are fewer than k spikes in a count window of size T is the same as the probability that the kth order interval is greater than T. The count distribution and interval distribution are therefore related by:

$$\hat{C}_T(k) = \begin{cases} \sum_{j=1}^{T} I_k(j) - I_{k+1}(j), & k \ge 1, \\ \sum_{j=1}^{T} I_1(j), & k = 0. \end{cases} \tag{14}$$

For a renewal process, the ISIs are independent and identically distributed with some known probability density function $I_1(j)$. Because any kth order interval of length r can be expressed as $r = \sum_{i=1}^{k} j_i$, where the j_i are the intervening ISIs, the renewality condi-

tion implies that the kth order interval distribution is the k-fold convolution of I_1 with itself (Feller, 1957). That is,

$$I_k(j) = \sum_{r=1}^{j-1} I_{k-1}(j - r) I_1(r), \, k > 1. \tag{15}$$

For renewal spike trains, we can use Equation 15 to express I_{k+1} in terms of I_k. Introducing this into Equation 14, and after some routine algebra, we have:

$$\hat{C}_T(k) = \sum_{r=k}^{T} \sum_{j=T+1}^{\infty} I_1(j - r) I_k(r). \tag{16}$$

From Equation 15 it can be seen that I_k is completely specified if I_1 is known, and hence, from Equation 16 count distributions are also known. That is, for a renewal process the ISI distribution I_1 is sufficient to completely describe the count distributions.

As an example, we can obtain the distribution of counts for a binomial spike train (Eq. 12) from the ISI distribution (Eq. 10). Repeated application of Equation 15 with I_1 the geometric density given by Equation 10 yields the kth order interval distribution given by Equation 11. Furthermore, inserting Equations 10 and 11 into Equation 16 yields the binomial distribution given by Equation 12.

For a nonrenewal process, the chief difficulty lies in relating the ISI distribution I_1 to the kth-order interval distributions. That is, neither the convolution expression given by Equation 15 nor the expression for count distribution given by Equation 16 are applicable. Therefore, Equation 14 can be evaluated only if I_k for all $k \ge 1$, are known. Thus, for a nonrenewal process, the ISI distribution does not provide information about counts or intervals on multiple time scales.

APPENDIX B

Measures of variability for renewal processes

Let I_1 be the ISI distribution for a renewal process, and let $\bar{I}_1$ and $\text{Var}(I_1)$ be its mean and variance, respectively. Then, as the kth-order interval is the sum of k independent random variables, the mean and variance of I_k are $k\bar{I}_1$ and $k \text{Var}(I_1)$, respectively. Thus, the coefficient of variation $\text{CV}_I(k)$ is:

$$\text{CV}_I(k) = \frac{1}{\sqrt{k}} \frac{\text{Var}(I_1)^{1/2}}{\bar{I}_1} = \frac{1}{\sqrt{k}} \text{CV}_I(1). \tag{17}$$

That is, the coefficient of variation decreases as $k^{-1/2}$. Likewise, the variance-to-mean ratio $F_I(k)$ is:

$$F_I(k) = \text{Var}(I_k)/\bar{I}_k = \text{Var}(I_1)/\bar{I}_1 = \text{constant.} \tag{18}$$

For the binomial model, it follows from Equation 11 that $\bar{I}_k = k/p$ and $\text{Var}(I_k) = k(1 - p)/p^2$. Therefore, $\text{CV}_I(k) = \sqrt{(1 - p)/k}$ and $F_I(k) = (1 - p)/p$.

For a nonrenewal process, $\text{Var}(I_k)$ can be related to $\text{Var}(I_1)$ and the correlation coefficients ρ_l by $\text{Var}(I_k) = k \text{Var}(I_1)\{1 + 2\sum_{l=1}^{k-1}(1 - (\frac{l}{k}))\rho_l\}$.

The coefficient of variation and Fano factor expressions for spike count distributions are more complicated than those for the intervals, with the exception of binomial (and Poisson) processes for which they are easily calculated. For the binomial spike train, it follows from Equation 12 that $\bar{C}_T = Tp$ and $\text{Var}(C_T) = Tp (1 - p)$. Thus, $\text{CV}_C(T) = \sqrt{(1 - p)/Tp}$, and falls as $T^{-1/2}$. The Fano factor $F_C(T) = 1 - p$, and is constant for all T. Any process with $F_C(T)$ smaller than this value will exhibit greater regularity in spike counts than the binomial process, and conversely, more irregular processes will have larger values.

For small T, $F_C(T)$ for any discrete time process will tend to $1 - p$ where p is the probability of firing in the sampling interval. That

is, for counting times $T \to 1$, the process is nearly binomial. For a continuous time process, when the count window $\Delta t \to 0$ then $p \to 0$. Thus, $F_C(T) \to 1$, which is the Fano factor for a Poisson process. That is, we expect spike counts in small count windows to be as irregular as a Poisson process. For renewal processes, the Fano factor for large T asymptotically approaches a constant value that is related to the coefficient of variation of the ISI by the relation, $F_C(T) \approx CV_I(1)^2$ (Cox and Lewis, 1966). That is, the variability of spike counts is attributable to the variability in interspike intervals.

REFERENCES

Amassian VE, Macy J, Waller HJ, Leader HS, Swift M (1964) Transformations of afferent activity at the cuneate nucleus. In: Information Processing in the Nervous System (Gerard RW, Duyff J, eds), pp 235–254. Amsterdam: Excerpta Medica Foundation.

Baddeley R, Abbott LF, Booth MCA, Sengpiel F, Freeman T, Wakeman EA, Rolls ET (1997) Responses of neurons in primary and inferior temporal visual cortices to natural scenes. Proc R Soc Lond B Biol Sci, 264:1775–1783.

Barlow HB, Levick WR (1969a) Changes in the maintained discharge with adaptation level in the cat retina. J Physiol (Lond) 202:699–718.

Barlow HB, Levick WR (1969b) Three factors limiting the reliable detection of light by the retinal ganglion cells of the cat. J Physiol (Lond) 200:1–24.

Bastian J (1981) Electrolocation. I. how the electroreceptors of *Apteronotus albifrons* code for moving objects and other electrical stimuli. J Comp Physiol [A] 144:465–479.

Bullock TH, Chichibu S (1965) Further analysis of sensory coding in electroreceptors of electric fish. Proc Natl Acad Sci USA 54:422–429.

Bullock TH, Heiligenberg W (1986) Electroreception. New York: Wiley.

Calvin WH, Stevens CF (1968) Synaptic noise and other sources of randomness in motoneuron interspike intervals. J Neurophysiol 31:574–587.

Cox DR (1962) Renewal theory. London: Methuen.

Cox DR, Lewis PAW (1966) The statistical analysis of series of events. London: Methuen.

Fano U (1947) Ionization yield of radiations. II. The fluctuations of the number of ions. Phys Rev 72:26–29.

Feller W (1957) An introduction to probability theory and its applications, Volume 1. New York: Wiley.

Gabbiani F, Koch C (1998) Principles of spike train analysis. In: Methods in neuronal modeling: from ions to networks (Koch C, Segev I, eds), pp 313–360. Cambridge: MIT.

Green D, Swets J (1966) Signal detection theory and psychophysics. New York: Wiley.

Hagiwara S (1954) Analysis of interval fluctuation of the sensory nerve impulse. Jpn J Physiol 4:234–240.

Hagiwara S, Morita H (1963) Coding mechanisms of electroreceptor fibers in some electric fish. J Neurophysiol 26:551–567.

Hagiwara S, Szabo T, Enger PS (1965) Electroreceptor mechanisms in a high-frequency weakly electric fish, *Sternarchus albifrons.* J Neurophysiol 28:784–799.

Hopkins CD (1976) Stimulus filtering and electroreception: tuberous electroreceptors in three species of gymnotid fish. J Comp Physiol [A] 111:171–207.

Johnson DH, Tsuchitani C, Linebarger DA, Johnson MJ (1986) Application of a point process model to responses of cat lateral superior olive units to ipsilateral tones. Hear Res 21:135–159.

Knudsen EI (1974) Behavioral thresholds to electric signals in high frequency electric fish. J Comp Physiol 91:333–353.

Kuffler SW, Fitzhugh R, Barlow HB (1957) Maintained activity in the cat's retina in light and darkness. J Gen Physiol 40:683–702.

Longtin A (1998) Firing dynamics of electroreceptors. In: Proceedings of the Fifth International Conference on Neural Information Processing, pp 27–30. Tokyo: IOP.

Longtin A, Racicot DM (1997a) Assessment of linear and nonlinear correlations between neural firing events. In: Nonlinear dynamics and time series: building a bridge between the natural and statistical sciences. Fields Institute Communications, Vol II. (Cutler CD, Kaplan DT, eds) pp 223–239. Providence, RI: American Mathematical Society.

Longtin A, Racicot DM (1997b) Spike train patterning and forecastability. BioSystems 40:111–118.

Lowen SB, Teich MC (1992) Auditory-nerve action potentials form a nonrenewal process over short as well as long time scales. J Acoust Soc Am 92:803–806.

Metzner W, Koch C, Wessel R, Gabbiani F (1998) Feature extraction by burst-like spike patterns in multiple sensory maps. J Neurosci 18:2283–2300.

Moore GP, Perkel DH, Segundo JP (1966) Statistical analysis and functional interpretation of neuronal spike data. Annu Rev Physiol 28:493–522.

Nakahama H, Ishii N, Yamamoto M (1972) Markov process of maintained impulse activity in central single neurons. Kybernetik 11:61–72.

Nelson ME, MacIver MA (1999) Prey capture in the weakly electric fish *Apteronotus albifrons*: sensory acquisition strategies and electrosensory consequences. J Exp Biol 202:1195–1203.

Nelson ME, Xu Z, Payne JR (1997) Characterization and modeling of p-type electrosensory afferent responses to amplitude modulations in a wave type electric fish. J Comp Physiol [A] 181:532–544.

Rasnow B (1996) The effects of simple objects on the electric field of *Apteronotus.* J Comp Physiol [A] 178:397–411.

Ratliff F, Hartline HK, Lange D (1968) Variability of interspike intervals in optic nerve fibres of limulus: effect of light and dark adaptation. Proc Natl Acad Sci USA 60:464–469.

Relkin EM, Pelli DG (1987) Probe tone thresholds in the auditory nerve measured by two-interval forced-choice procedures. J Acoust Soc Am 82:1679–1691.

Rodieck RW, Kiang NYS, Gerstein GL (1962) Some quantitative methods for the study of spontaneous activity of single neurons. Biophys J 2:351–368.

Scheich H, Bullock TH, Hamstra RH (1973) Coding properties of two classes of afferent nerve fibers: high frequency electroreceptors in the electric fish, *Eigenmannia.* J Neurophysiol 36:39–60.

Shadlen M, Newsome WT (1998) The variable discharge of cortical neurons: implications for connectivity, computation, and information coding. J Neurosci 18:3870–3896.

Shannon CE (1948) The mathematical theory of communication. Bell Syst Tech J 27:379–423, 623–656.

Shofner WP, Dye RH (1989) Statistical and receiver operating characteristic analysis of empirical spike count distributions: quantifying the ability of cochlear nucleus units to signal intensity changes. J Acoust Soc Am 86:2172–2184.

Shumway CA (1989) Multiple electrosensory maps in the medulla of weakly electric gymnotiform fish. I. physiological differences. J Neurosci 9:4388–4399.

Softky WR, Koch C (1993) The highly irregular firing of cortical cells is inconsistent with temporal integration of random EPSPs. J Neurosci 13:334–350.

Teich MC, Khanna SM (1985) Pulse-number distribution for the neural spike train in the cat's auditory nerve. J Acoust Soc Am 77:1110–1128.

Teich MC, Johnson DH, Kumar AR, Turcott RG (1990) Rate fluctuations and fractional power-law noise recorded from cells in the lower auditory pathway of the cat. Hear Res 46:41–52.

Teich MC, Turcott RG, Siegel RM (1996) Temporal correlation in cat striate-cortex neural spike trains. IEEE Eng Med Biol 15:79–87.

Teich MC, Heneghan C, Lowen SB, Ozaki T, Kaplan E (1997) Fractal character of the neural spike train in the visual system of the cat. J Opt Soc Am A 14:529–546.

Tuckwell HC (1988) Introduction to theoretical neurobiology, Vol. 2. New York: Cambridge UP.

van der Heyden MJ, Diks CGC, Hoekstra BPT, DeGoede J (1998) Testing the order of discrete Markov chains using surrogate data. Physica D 117:299–313.

Werner G, Mountcastle VB (1963) The variability of central neural activity in a sensory system, and its implications for the central reflection of sensory events. J Neurophysiol 26:958–977.

Wessel R, Koch C, Gabbiani F (1996) Coding of time-varying electric field amplitude modulations in a wave-type electric fish. J Neurophysiol 75:2280–2293.

Xu Z, Payne JR, Nelson ME (1996) Logarithmic time course of sensory adaption in electrosensory afferent nerve fibers in a weakly electric fish. J Neurophysiol 76:2020–2032.

Young ED, Barta PE (1986) Rate responses of auditory nerve fibers to tones in noise near masked threshold. J Acoust Soc Am 79:426–442.

Zakon HH (1986) The electroreceptive periphery. In: Electroreception (Bullock TH, Heiligenberg W, eds), pp 103–105. New York: Wiley.